Journal of Alloys and Compounds 509 (2011) 1178–1186

Contents lists available at ScienceDirect

Journal of Alloys and Compounds

journal homepage: www.elsevier.com/locate/jallcom

Formation of macroscopically phase separated Cu-colored melt-spun ribbon in $(Fe_{0.5}Cu_{0.5})_{100-x}B_x$ ($x = 0$, 5, 10, and 20) alloys

Takeshi Nagase[a,b,*], Akimasa Yokoyama[b], Yukichi Umakoshi[c]

[a] Research Center for Ultra-High Voltage Electron Microscopy, Osaka University, 7-1, Mihogaoka, Ibaraki, Osaka 567-0047, Japan
[b] Division of Materials and Manufacturing Science, Graduate School of Engineering, Osaka University, 2-1, Yamada-Oka, Suita, Osaka 565-0871, Japan
[c] National Institute for Materials Science, 1-2-1, Sengen, Tsukuba, Ibaraki 305-00471, Japan

ARTICLE INFO

Article history:
Received 6 August 2010
Received in revised form
19 September 2010
Accepted 26 September 2010
Available online 28 October 2010

Keyword:
Rapid solidification

ABSTRACT

The microstructure of a rapidly solidified melt-spun ribbon of binary Fe–Cu and ternary Fe–Cu–B alloys was investigated. The duplex structure composed of Fe–B-rich and Cu-rich alloys was formed by liquid phase separation of Fe–Cu–B alloys regardless of the B content. We found that the element Cu shows a strong tendency to segregate on the surface of Fe–Cu–B alloy ribbons, resulting in the formation of a macroscopically phase-separated Cu-colored cover layer/core structure.

© 2010 Elsevier B.V. All rights reserved.

1. Introduction

It is important to improve existing material processing methods in order to develop new metallic materials with superior structural and functional properties because these materials can play an important role in the sustainable development of human society and the maintenance of the natural environment. In particular, it is well known that the rapid solidification technique can be effectively used to develop new materials. Rapid solidification leads to the formation of a metastable phase, which cannot be obtained by conventional material processes (for example, the formation of an amorphous phase). Furthermore, rapid solidification can be used to change the material's solidification mode (for example, from eutectic to dendrite solidification mode) and for the suppression of segregation, structural refinement, liquid phase separation, and so on. Recently, the formation of a unique solidification structure in a rapidly solidified melt-spun ribbon was reported for alloys that underwent simultaneous liquid phase separation and an amorphous phase formation [1–13]. The formation of nano-scale emulsion-type structures (nano-scale globule-dispersed structures), multi-scale globule-dispersed structures, marble-type structures (entangled duplex structures), macroscopically phase-separated dual-layer structures, etc. has been reported. Melt-spun ribbons of alloys undergoing liquid phase separation during rapid solidification offer new possibilities for the formation of a unique solidification structure which cannot be obtained by conventional material processes

It is well known that the Fe–Cu alloy system shows a metastable liquid miscibility gap below the liquidus; the formation of this gap can be attributed to the large heat of mixing of the Fe–Cu pair [14–27]. In this paper, we report the preparation of a rapidly solidified melt-spun ribbon of binary Fe–Cu and ternary Fe–Cu–B alloys with different values of B concentration. This is the first time that the formation of a macroscopically phase-separated Cu-colored melt-spun ribbon, namely, a continuous melt-spun ribbon with a Cu-colored Cu-crystalline cover layer/core structure has been reported.

2. Experimental procedures

Master ingots of $Fe_{50}Cu_{50}$ and $(Fe_{0.5}Cu_{0.5})_{100-x}B_x$ ($x = 5$, 10, and 20) alloys were prepared from Fe, Cu, B, and Fe–B on a water-cooled Cu hearth by arc melting in purified Ar atmosphere. Rapidly quenched ribbons with a cross section of about 3.0 mm × 0.04 mm were produced from the master alloys ingots by means of a single-roller melt-spinning method. The melt-spinning quenching apparatus with a 200 mm diameter copper roller operated also in an Ar atmosphere. The rotation speed of the roller was set to 4000 min^{-1} so that the roller surface velocity was approximately 42 ms^{-1}. A quartz crucible with a diameter of 14 mm and an orifice of approximately 1.0 mm were used. We ensured that the gap between the crucible bottom and roller surface did not exceed 0.4 mm. The quantity of master alloys melting per run was estimated to be approximately 10 g. The pressure of the gas ejected was 0.06 MPa. In the case of Fe–Cu–B alloys, it was impossible to eject all thermal melt into the quartz crucible and residual ingots were produced. The structure of the final melt-spun ribbon was examined by X-ray diffractometry (XRD) using a Cu Kα radiation, an optical microscopy (OM), back-scattering electron image (BEI) of scanning electron microscopy (SEM), and electron probe microanalysis (EPMA). Thermal properties of the ribbon were determined by differential scanning calorimetry (DSC) and differential thermal analysis (DTA).

* Corresponding author at: Research Center for Ultra-High Voltage Electron Microscopy, Osaka University, 7-1, Mihogaoka, Ibaraki, Osaka 567-0047, Japan. Tel.: +81 6 6879 7941; fax: +81 6 6879 7942.
E-mail address: t-nagase@uhvem.osaka-u.ac.jp (T. Nagase).

0925-8388/$ – see front matter © 2010 Elsevier B.V. All rights reserved.
doi:10.1016/j.jallcom.2010.09.168

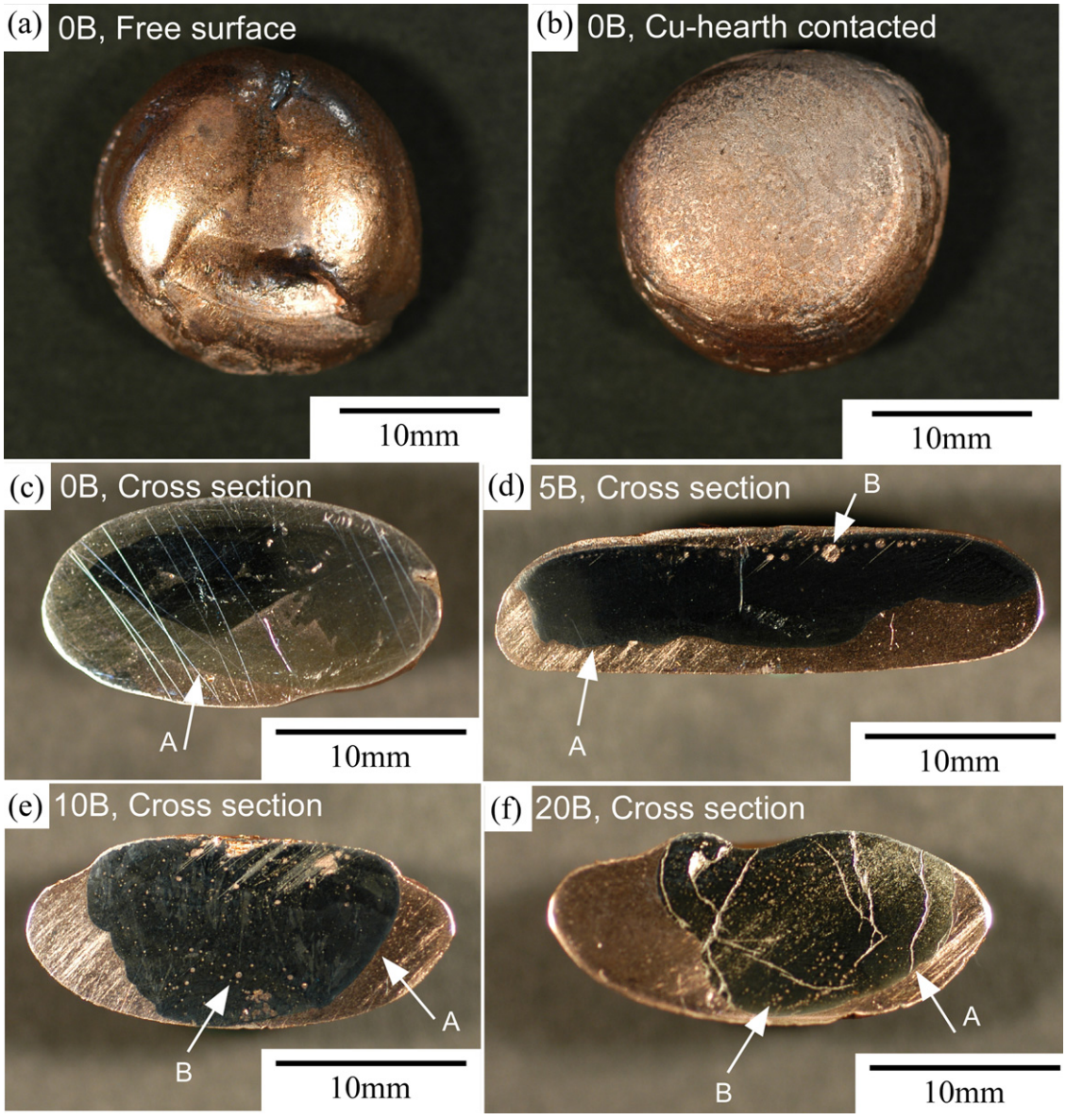

Fig. 1. Optical micrographs of free surface of $Fe_{50}Cu_{50}$ ingot (a); Cu hearth contacted side surface of $Fe_{50}Cu_{50}$ ingot (b), and cross section of slowly solidified $Fe_{50}Cu_{50}$ (c), $Fe_{47.5}Cu_{47.5}B_5$ (d), $Fe_{45}Cu_{45}B_{10}$ (e), and $Fe_{40}Cu_{40}B_{20}$ ingot (f) obtained by arc-melting.

3. Results

Fig. 1 shows optical micrographs of the free surface (a), the Cu hearth contacted side surface (b), and the cross section ((c)–(f)) in slowly solidified ingots prepared by arc melting. In the cross-sectional images, the lower part of the images corresponds to the Cu hearth contacted side. As shown in Fig. 1(a) and (b), $Fe_{50}Cu_{50}$ ingots did not have the metallic silver color surface, which is typical for conventional metals, but a Cu-colored surface. Cu-colored ingots were also obtained from ternary Fe–Cu–B alloys. In the cross-sectional images, one can notice a distinctive core–shell structure, which is particularly pronounced in Fe–Cu–B alloys ingots. The core region has a metallic silver color, while the shell region is Cu-colored. The interface between the metallic silver core and Cu-colored shell is extremely smooth, as indicated by index A. Furthermore, Cu-colored globules were observed in the metallic silver core matrix, and a typical example of these structures is indicated by index B. These globules were observed in the case of the ternary Fe–Cu–B alloy regardless of its composition. Fig. 2 shows the cooling DTA curves for the thermal melt of binary Fe–Cu and ternary Fe–Cu–B alloys. The melt with an initial temperature of 1773 K was cooled down at a rate of 0.33 $K\,s^{-1}$. The two peaks observed in the exothermic heat release in binary Fe–Cu and ternary Fe–Cu–B alloys are indicated by arrows. The position of these two exothermic peaks indicates the strong dependence on the composition of the alloys. Furthermore, the temperature at which the two exothermic peaks are observed is lower than the melting temperature of pure-Fe (T_m(Fe)). The two exothermic peaks provide proof of the separate solidification of each liquid after the liquid phase separation. These results suggest that liquid phase separation occurred in binary Fe–Cu as well as ternary Fe–Cu–B alloys and resulted in the formation of a structure with a Fe-rich alloy core and a Cu-rich alloy shell.

Fig. 3 shows the outer appearance of the rapidly solidified melt-spun ribbon of binary Fe–Cu and ternary Fe–Cu–B alloys. The $Fe_{50}Cu_{50}$ alloy ribbon has a flake-like shape and a metallic silver color surface, while the ternary Fe–Cu–B alloy ribbon with a Cu-colored surface is continuous. The addition of B in binary Fe–Cu alloy has proven to be effective in improving its ability to form a continuous melt-spun ribbon. Fig. 4 shows optical micrographs of

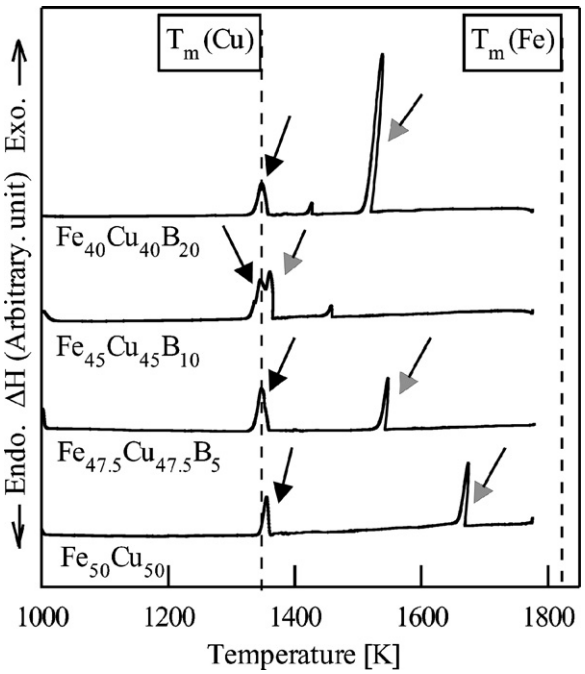

Fig. 2. Cooling DTA curves of thermal melt of binary Fe–Cu and ternary Fe–Cu–B alloys. The melt with an initial temperature of 1773 K was cooled down at a rate of 0.33 K s^{-1}.

the free surface ((a)–(d)) and roll-side surface ((e) and (f)) of the rapidly solidified melt-spun ribbon of binary Fe–Cu and ternary Fe–Cu–B alloys. An extremely smooth surface without the typical roughness of an amorphous ribbon was not observed. The free surface of ternary Fe–Cu–B alloy melt-spun ribbons has a Cu-colored surface, while the binary Fe–Cu alloy melt-spun ribbon has a metallic silver color surface. On roll-side surface (Fig. 4(e) and (f)), the duplex structure of the Cu- and metallic silver-colored region can be seen in case of ternary Fe–Cu–B alloys; the white arrows indicate the boundary between Cu- and metallic silver-colored region. In spite of the relatively small extent of metallic silver-colored region on the roll-side surface, the melt-spun ribbon of ternary Fe–Cu–B alloy exhibits a strong tendency for a Cu-colored surface. Fig. 5 shows optical micrographs of the cross section and surface structures on the rapidly solidified melt-spun ribbon of ternary Fe–Cu–B alloys. These cross-sectional and surface images were obtained simultaneously because the specimens are embedded in transparent resin. Both the $Fe_{47.5}Cu_{47.5}B_5$ (Fig. 5(a)) and $Fe_{45}Cu_{45}B_{10}$ (Fig. 5(b)) alloy ribbon have a duplex structure composed of a Cu-colored region and a metallic silver-colored region. In particular, the metallic silver-colored region can also be seen in the internal part of the melt-spun ribbon of $Fe_{40}Cu_{40}B_{20}$ alloy (c). There is a significant difference between the outer and internal part of the rapidly solidified melt-spun ribbon of ternary Fe–Cu–B alloy. A macroscopically phase-separated structure, namely, a Cu-colored surface layer/metallic silver-colored or marble-type core structure can be seen.

XRD, DSC, SEM, and EPMA analyses were performed on the melt-spun ribbon, in order to investigate in more detail the macroscopically phase-separated structure in detail. Fig. 6 shows the XRD patterns of the rapidly solidified melt-spun ribbon of binary Fe–Cu and ternary Fe–Cu–B alloys. XRD patterns were observed on the free surface, roll-side surface and internal part (in the case of a polished sample). Although the penetration depth of X-rays can be several tens of micrometers, XRD offers the opportunity to clarify the differences between the surface and the internal regions of the

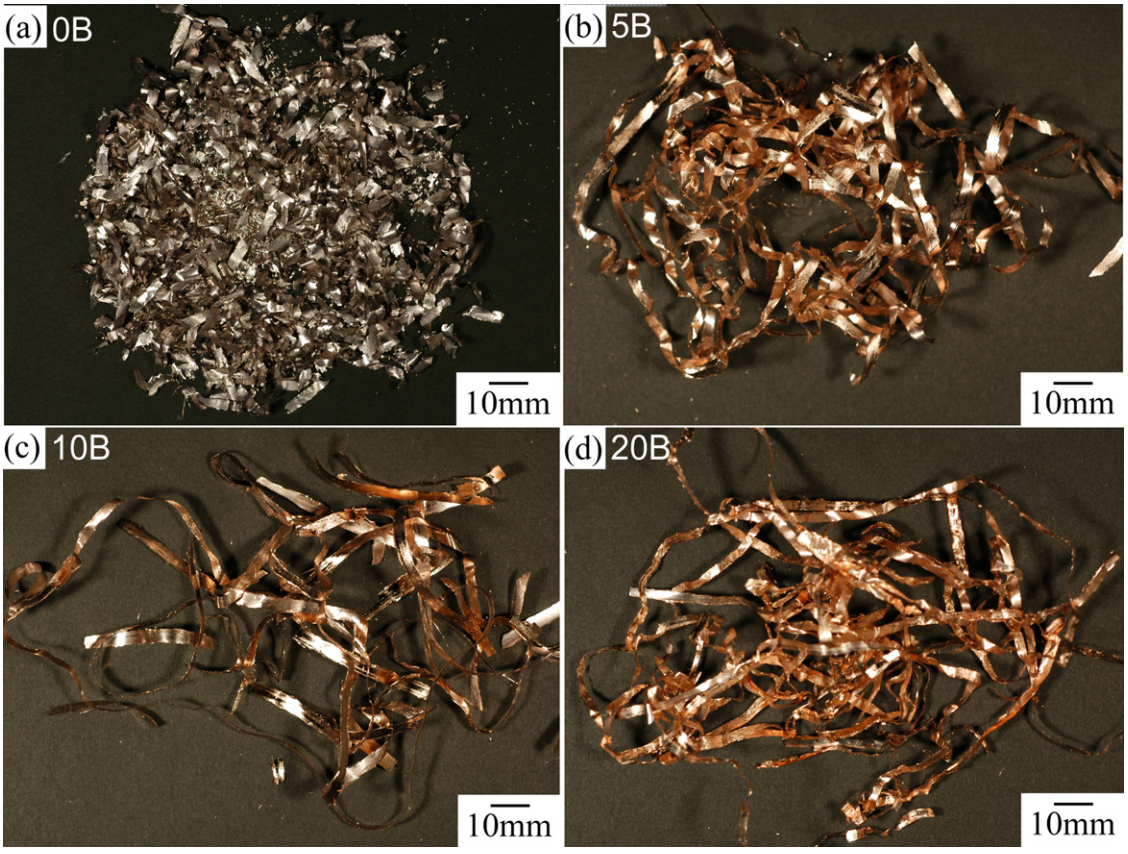

Fig. 3. Outer appearance of rapidly solidified melt-spun ribbons of four different binary Fe–Cu and ternary Fe–Cu–B alloys: (a) $Fe_{50}Cu_{50}$, (b) $Fe_{47.5}Cu_{47.5}B_5$, (c) $Fe_{45}Cu_{45}B_{10}$, (d) $Fe_{40}Cu_{40}B_{20}$.

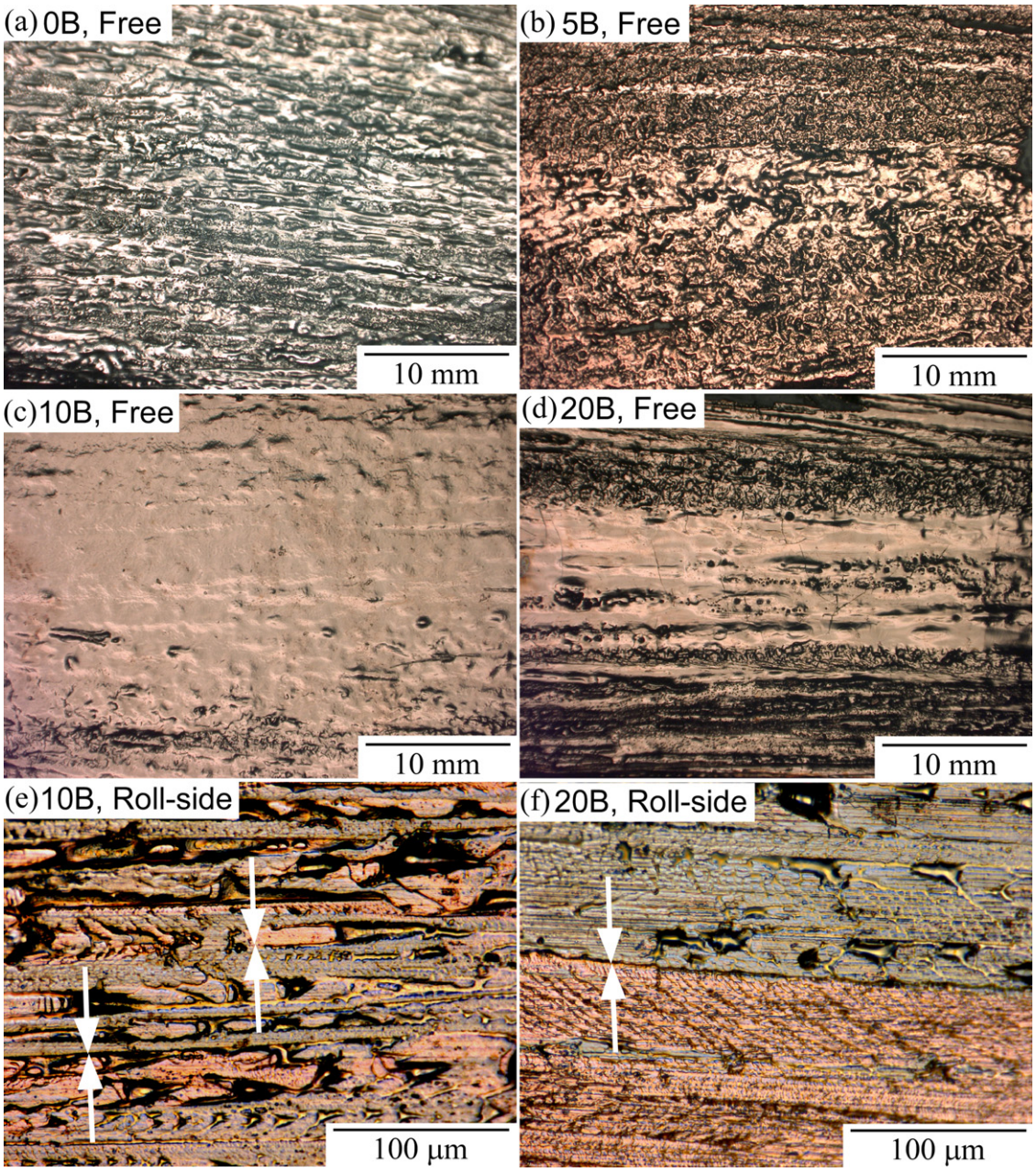

Fig. 4. Optical micrographs of free surface of rapidly solidified melt-spun ribbon made of $Fe_{50}Cu_{50}$ (a), $Fe_{47.5}Cu_{47.5}B_5$ (b), $Fe_{45}Cu_{45}B_{10}$ (c) and $Fe_{40}Cu_{40}B_{20}$ (d), and roll-side surface of $Fe_{45}Cu_{45}B_{10}$ (e) and $Fe_{47.5}Cu_{47.5}B_5$ alloy ribbon (f). White arrows indicate the boundary between Cu- and metallic silver-colored region.

alloy ribbon. Both the $Fe_{50}Cu_{50}$ (Fig. 6(a)) and the $Fe_{47.5}Cu_{47.5}B_5$ (Fig. 6(b)) alloy shows sharp diffraction peaks corresponding to alpha iron (α-Fe) and Cu crystalline phases. A significant difference observed between the free surface, roll-side surface and internal part cannot be seen. On the other hand, both in the case of the $Fe_{45}Cu_{45}B_{10}$ (Fig. 6(c) and (e)) and the $Fe_{40}Cu_{40}B_{20}$ alloys (Fig. 6(d)), sharp diffraction peaks can be seen which correspond to the Cu crystalline phase. However, the intensity of the peak corresponding to alpha iron is much smaller than that in the case of $Fe_{50}Cu_{50}$ and $Fe_{47.5}Cu_{47.5}B_5$ alloys. As shown in Fig. 6(e), Fe–B intermetallic compounds such as FeB and Fe_3B seem to be formed in the case of $Fe_{45}Cu_{45}B_{10}$ and $Fe_{40}Cu_{40}B_{20}$ alloys. One can also notice that the peak corresponding to alpha iron can be observed only in the case of a polished sample in spite of the absence of such a crystalline phase on the free surface and the roll-side surface of a $Fe_{40}Cu_{40}B_{20}$ alloy ribbon. The Cu-colored surface layer/metallic silver-colored core structure, namely, the Cu crystalline phase cover layer/Fe-based alloy core structure was observed on the $Fe_{40}Cu_{40}B_{20}$ alloy ribbon. DSC analysis did not show any exothermic peak corresponding to the crystallization of an amorphous phase. Both XRD and DSC indicates that no amorphous phase is formed in the melt-spun ribbon.

Figs. 7 and 8 show SEM–BEI micrographs on the rapidly solidified melt-spun ribbon of binary Fe–Cu and ternary Fe–Cu–B alloys and the results of the EPMA. The observation direction is perpendicular to the ribbon surface. The duplex structure composed of dark and bright gray regions can be seen in Fig. 8. The dark and bright gray regions are enriched with Fe and Cu, respectively. In addition the Fe-rich region is also enriched with B, which is absent in Cu-rich region of the ternary Fe–Cu–B alloy ribbon. The results of both SEM and EPMA indicate that the entangled duplex structure composed of Fe–B- and Cu-rich phases was the result of single-

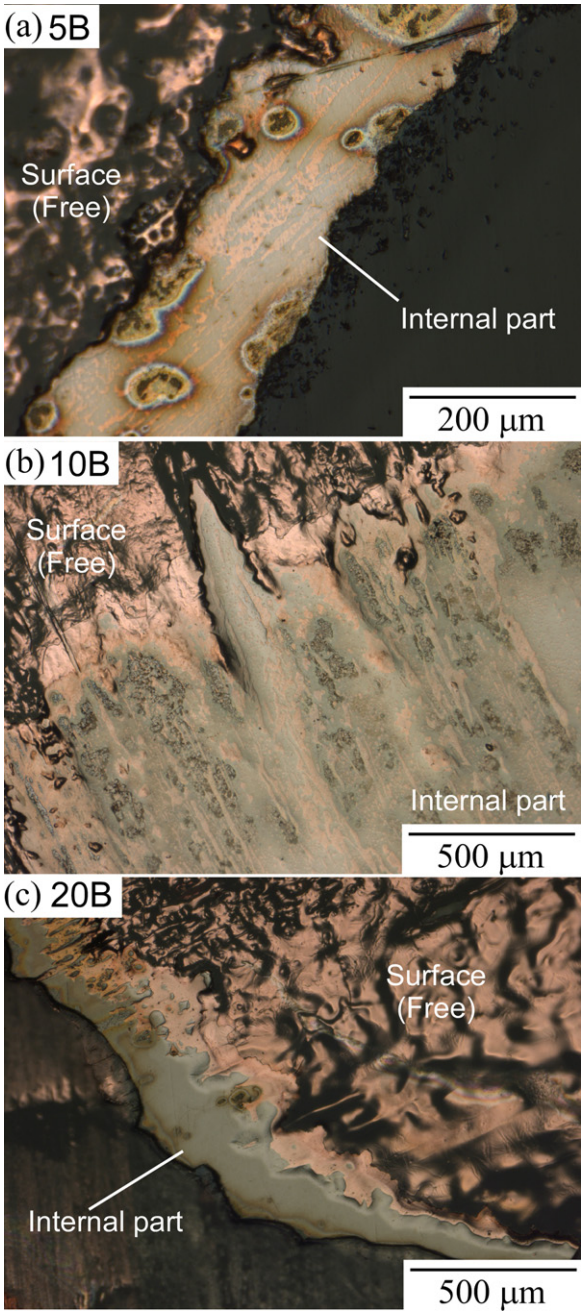

Fig. 5. Optical micrographs of cross section and outer surface of rapidly solidified melt-spun ribbon of ternary Fe–Cu–B alloys. The cross section and surface images were obtained simultaneously because the specimens were embedded in transparent resin: (a) $Fe_{47.5}Cu_{47.5}B_5$, (b) $Fe_{45}Cu_{45}B_{10}$, (c) $Fe_{40}Cu_{40}B_{20}$.

roller melt spinning of the ternary Fe–Cu–B alloy. The sizes of Fe- and Cu-rich alloy regions were found to increase with increasing B content. The smooth interface between the Fe- and Cu-rich alloy regions, and the globule phases, which are typical features of liquid phase separation, can be seen in ternary Fe–Cu–B alloy ribbon. A marble-type entangled-duplex structure can be seen in the case of the $Fe_{47.5}Cu_{47.5}B_5$ (Fig. 7(b)) and $Fe_{45}Cu_{45}B_{10}$ alloy (Fig. 7(c)). In addition, a structure resembling to a backwater liquid flow can be seen in the $Fe_{47.5}Cu_{47.5}B_5$ alloy ribbon (Fig. 7(f)). Such a unique structure has never been reported in rapidly solidified ribbons of alloys, which have undergone simultaneously liquid phase separation and amorphous phase formation [1–13]. On the $Fe_{40}Cu_{40}B_{20}$ alloy ribbon (Fig. 8(g)), a dark contrast region can be seen within a white region, and gray regions of varying contrast. These formations may be attributed to the formation of intermetallic compounds. While their internal structure is highly dependent on the B content, the crystalline Cu layer can be seen regardless of the B content.

Fig. 9 shows SEM micrographs of the cross section of the rapidly solidified melt-spun ribbon. The cross-sectional images of the $Fe_{45}Cu_{45}B_{10}$ (Fig. 9(a)) and the $Fe_{40}Cu_{40}B_{20}$ (Fig. 9(b)) provide evidence of the separation of Fe-rich region from the Cu-rich region, where the morphology of solidification structure is different from that shown in Fig. 7. The segregation of Cu from within the alloy ribbon to outer surface can also be confirmed. The extent of the Cu-rich region on the ribbon's free surface seems to be larger than that in roll-side surface, which is good agreement with the optical micrographs of free surface and roll-side surface shown in Fig. 4. In the case of the $Fe_{45}Cu_{45}B_{10}$ alloy ribbon (Fig. 9(a)), not only a macroscopically phase-separated core/cover layer structure but also microscopically phase-separated marble-type structure can be seen within the core region. In contrast, the formation of marble-type structure cannot be seen in the core region of the $Fe_{40}Cu_{40}B_{20}$ alloy ribbon (Fig. 9(b)). The B content seems to affect the solidification structure formed by liquid phase separation; however, the macroscopically phase-separated was observed in the ternary Fe–Cu–B alloy ribbon regardless the B content. A Cu-colored cover layer/marble core structure was formed in both $Fe_{47.5}Cu_{47.5}B_5$ and $Fe_{45}Cu_{45}B_{10}$ alloy ribbons, while the Cu-colored cover layer/metallic silver-colored core layer structure was observed in the $Fe_{40}Cu_{40}B_{20}$ alloy ribbon.

4. Discussion

The macroscopically phase-separated structure composed of Fe-rich and Cu-rich regions was observed in slowly solidified arc-melted ingots. The addition of B has proven to be effective in separating Fe from Cu [27], which results in the formation of a Fe-rich core and a Cu-rich shell in the ingots. Tanaka et al. reported on the formation of a Fe core/Cu shell structure in bulk Fe–Cu–C alloy samples using specialized crucibles [28], while, in the case of Fe–Cu–B alloys, the core/shell structure can be obtained by the conventional arc-melt technique described in this paper. A similar egg-like structure has been observed in rapidly solidified powders prepared by gas-atomizing Fe–Cu–Si–C alloys [25]. The formation of the egg-like structure was attributed to the Marangoni convection observed after the separation of two melts. The difference between the surface energies of the Fe–B- and Cu-rich alloy liquids as well as the Marangoni convection of the liquids may be affecting the formation of the core–shell structure. Sufficient macroscopic transportation and/or diffusion of the order of millimeters during the solidification process can lead to the formation of a macroscopically phase-separated core–shell structure. During the cooling of the thermal melt on the Cu hearth, the liquid phase separation of Fe–B-based and the Cu-rich liquids occurs first; subsequently, the liquid aggregation results in the formation of macroscopically phase-separated core/shell structures.**

During rapid solidification, a unique macroscopically phase separated core/cover layer structure was formed by employing the single-roller melt-spinning method. To the best of our knowledge, this is the first report on the formation of macroscopically phase separated core/cover layer using a melt-spinning method. Another type of macroscopically phase separated dual-layer structure has been reported in previous paper, and the formation mechanism has been discussed in detail [13]. There are several factors that govern the formation of the core/cover layer structure: (1) homogeneous and inhomogeneous melt ejection, (2)

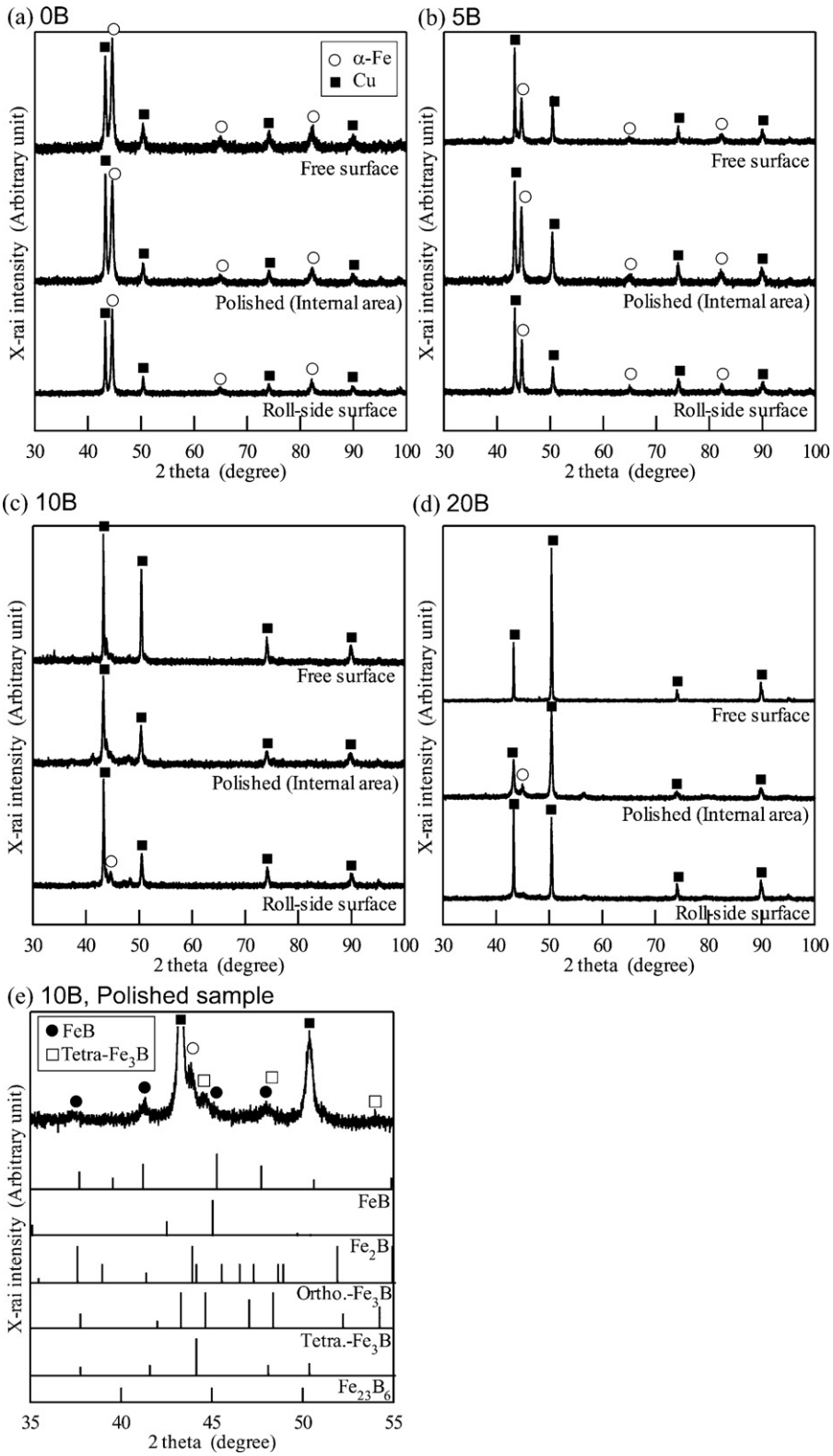

Fig. 6. XRD patterns of rapidly solidified melt-spun ribbon made of binary Fe–Cu and ternary Fe–Cu–B alloys. XRD patterns observed on free and roll-side surface and in interior of polished sample: (a) $Fe_{50}Cu_{50}$, (b) $Fe_{47.5}Cu_{47.5}B_5$, (c) $Fe_{45}Cu_{45}B_{10}$, (d) $Fe_{40}Cu_{40}B_{20}$, and (e) polished sample made of $Fe_{45}Cu_{45}B_{10}$.

homogeneous and inhomogeneous nucleation on the Cu wheel, (3) difference between the cooling rates of the roll-side and free surfaces, (4) difference between the densities of the Cu-rich and Fe–B-rich alloy phases, (5) difference between the viscosities of the Cu-rich and F–B-rich alloy phases, (6) difference between the surface energies of the Cu-rich and Fe–B-rich alloy phases, (7) difference between the interface energies between the various melts and the wheel material (Cu), (8) oxidation of the surface layer, (9) volume ratio between Cu-rich and Fe–B-rich alloy phases, and so on. Among the abovementioned factors, homogeneous and

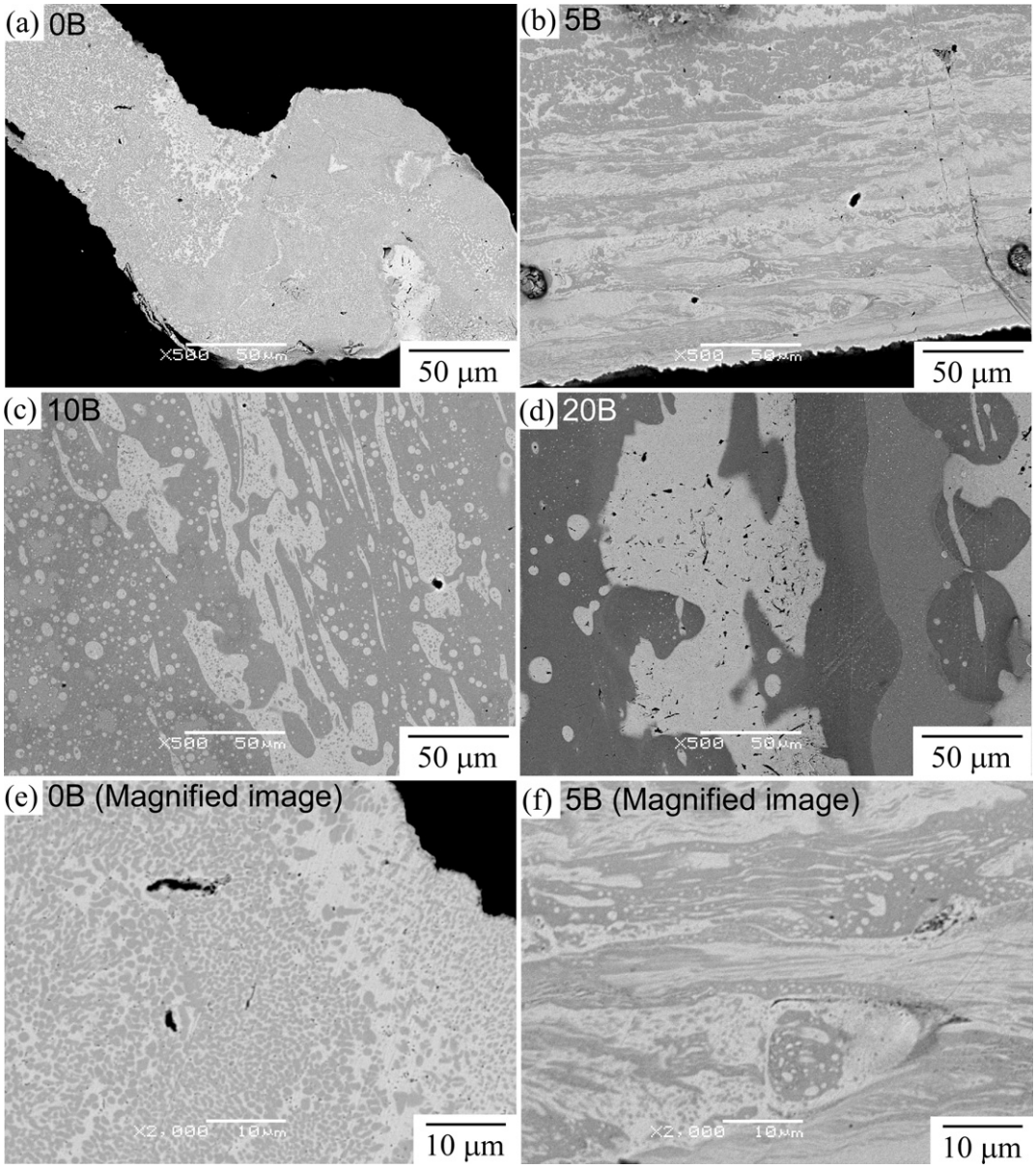

Fig. 7. SEM micrograph of rapidly solidified melt-spun ribbon made of binary Fe–Cu and ternary Fe–Cu–B alloys. The observation direction was perpendicular to the ribbon surface. The images is actually a back-scattering electron image (BEI) of the (a) $Fe_{50}Cu_{50}$, (b) $Fe_{47.5}Cu_{47.5}B_5$, (c) $Fe_{45}Cu_{45}B_{10}$, (d) $Fe_{40}Cu_{40}B_{20}$ alloy ribbon, or a magnified image of the $Fe_{50}Cu_{50}$ (e), and $Fe_{47.5}Cu_{47.5}B_5$ alloy ribbon (f).

inhomogeneous melt ejection can be considered to be the most important.

It is well known that melt spinning is associated with extremely high cooling rates of the order of 1×10^5 or 1×10^6 K s^{-1} [29]. Therefore, it would be difficult to achieve a sufficient level of macroscopic transportation and/or diffusion to form the core/cover layer structure because of the relatively short solidification time. One may considered that the application of the inhomogeneous liquid ejection model is reasonable in the present study only from the viewpoint of macroscopic transportation and/or diffusion. It has been reported in previous studies that the addition of B is more effective in separating Fe from Cu than the addition of C, P, or Si. The isothermal cross-sectional phase diagram of the Fe–Cu–B ternary system at 1873 K indicates that $(Fe_{0.5}Cu_{0.5})_{100-x}B_x$ (x = 0, 5, 10, and 20) alloys have two liquid phase regions [27]. In the case of ternary Fe–Cu–B alloys, the thermal melt consists of Fe–B-rich and Cu-rich liquids before it is ejected into the quartz crucible. Once this melt is ejected, the Cu-rich liquid is segregated during free flight in the Ar atmosphere and is finally aggregated on the surface layer. Consequently, the macroscopically phase-separated core/cover layer structure is formed. However, the inhomogeneous ejection model cannot suitably explain the unique macroscopically phase separated structure. In the case of the inhomogeneous liquid ejection model, the core/cover layer structure may be formed only contingently. The formation of this core/cover layer structure by the conventional single roller melt-spinning method cannot be explained only by the inhomogeneous liquid ejection model.

It is well known that the Fe–B binary alloy system forms an amorphous phase upon rapid solidification [30,31]. This indicates that the Fe–B liquid can maintain its liquid structure longer than conventional alloys without undergoing an amorphous phase formation. In the present study, Fe–B-rich and Cu-rich liquids were formed from the Fe–Cu–B alloy. The Fe–B liquid formation may

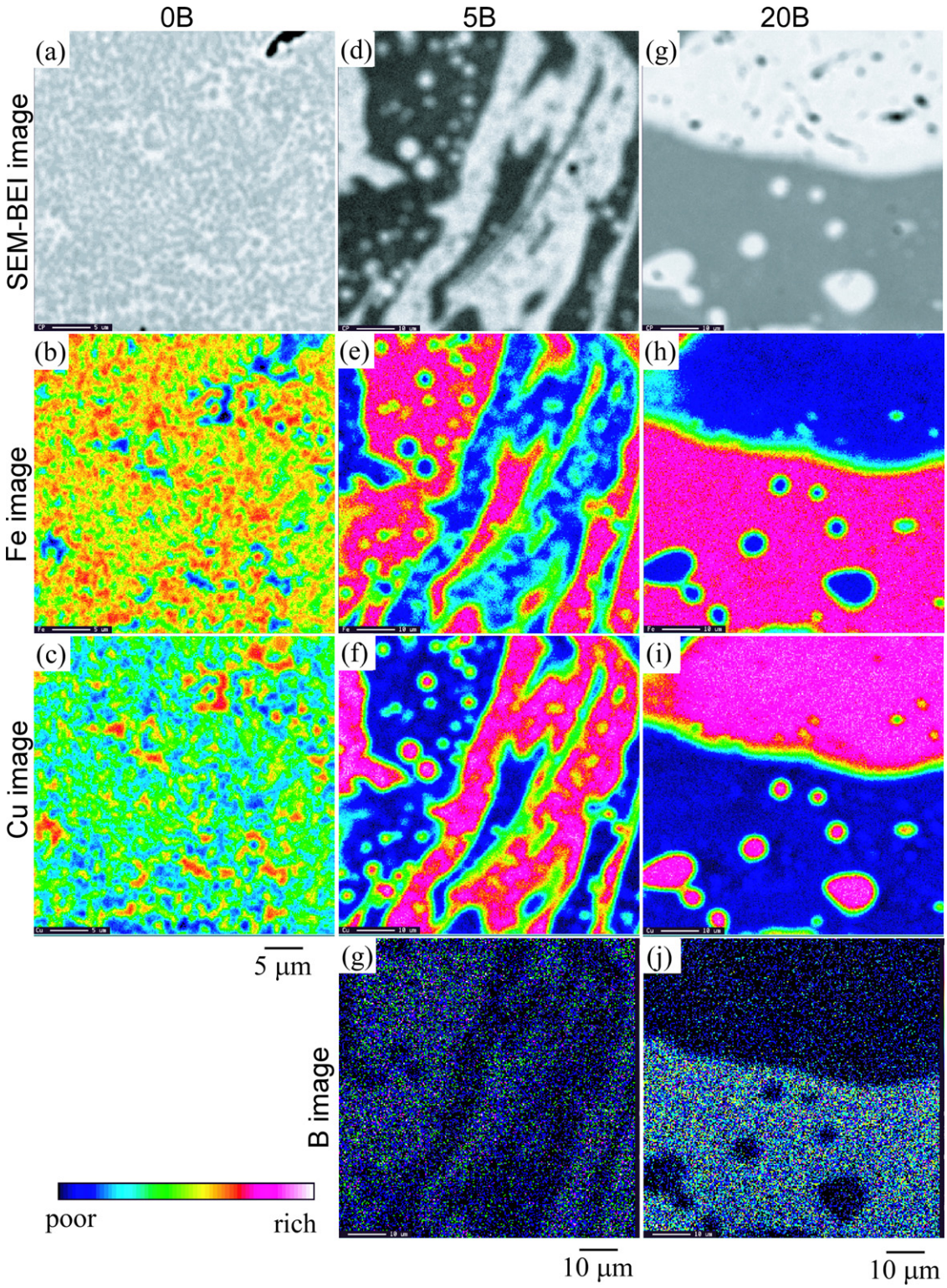

Fig. 8. Results of EPMA of rapidly solidified melt-spun ribbon made of $Fe_{50}Cu_{50}$ ((a), (b), and (c)), $Fe_{45}Cu_{45}B_{10}$ ((d), (e), (f), and (g)) and $Fe_{40}Cu_{40}B_{20}$ ((h), (i), (j), and (k)) alloys. The observation direction is perpendicular to the ribbon surface. ((a), (d), and (h)) BEI, ((b), (e), and (f)) Fe image, ((c), (f), and (j)) Cu image, and ((g), and (k)) B image.

be sufficiently effective in maintaining the liquid state during melt-spinning and free flight so that the alloy liquids experience Marangoni motion during the formation of the core/cover structure. The inhomogeneous liquid ejection and/or the Marangoni motion of Fe–B-rich (amorphous phase former type) and Cu-rich liquids may explain the formation of this unique macroscopically phase separated dual-layer structure. However, presently, the mechanism is unclear; we can only conclude that this structure was formed by liquid phase separation during the rapid quenching of the thermal melt. The mechanism governing the formation of the core/cover layer structure will be discussed in subsequent papers.

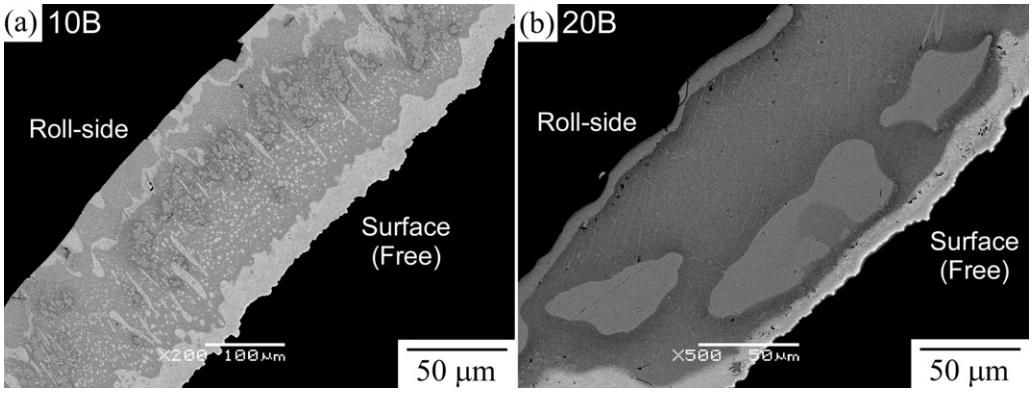

Fig. 9. SEM micrograph of cross section of rapidly solidified melt-spun ribbons made of two different ternary Fe–Cu–B alloys: (a) $Fe_{45}Cu_{45}B_{10}$, and (b) $Fe_{40}Cu_{40}B_{20}$. These cross section images are obtained at an angle that allowed us to easily observe the internal structure of the alloy ribbon.

5. Conclusions

In the present study, a rapidly solidified melt-spun ribbon of Fe–Cu and Fe–Cu–B alloys was prepared using single-roller melt spinning, and its microstructure was thoroughly investigated. The following conclusions were drawn:

(1) The addition of B in Fe–Cu alloy is effective in improving it ability to form a continuous melt-spun ribbon.
(2) A continuous melt-spun ribbon with a Cu-colored surface was obtained by the conventional single-roller melt spinning method in a ternary Fe–Cu–B alloy. Cu showed a strong tendency to segregate on the surface of the ribbon, resulting in the formation of macroscopically phase-separated Cu-colored cover layer/core structure.
(3) A unique solidification microstructures such as marble-type entangled-duplex structures and/or nano-scale emulsion-type structures, which cannot be obtained by conventional alloys, were formed in the core region of Fe–Cu–B alloy ribbons.

Acknowledgment

This study was supported by the Priority Assistance for the Formation of Worldwide Renowned Centers of Research—The Global COE Program (Project: Center of Excellence for Advanced Structural and Functional Materials Design) from the Ministry of Education, Culture, Sports, Science and Technology (MEXT), Japan.

References

[1] A.A. Kündig, M.D. Ohnuma, H. Ping, T. Ohkubo, K. Hono, Acta Mater. 52 (2004) 2441–2448.
[2] B.J. Park, H.J. Chang, D.H. Kim, W.T. Kim, Appl. Phys. Lett. 85 (2004) 6353–6355.
[3] N. Mattern, U. Kuhn, A. Gebert, T. Gemming, M. Zinkevich, H. Wendrock, L. Schultz, Scr. Mater. 53 (2005) 271–274.
[4] I. Yamauchi, T. Irie, H. Sakaguchi, J. Alloys Compd. 403 (2005) 211–216.
[5] T. Nagase, A. Yokoyama, Y. Umakoshi, Mater. Trans. 47 (2006) 1105–1114.
[6] T. Koziel, Z. Kedzierski, A. Zielińska-Lipiec, K. Ziewiec, Scr. Mater. 54 (2006) 1991–1995.
[7] E.S. Park, D.H. Kim, Acta Mater. 54 (2006) 2597–2604.
[8] K. Ziewiec, Z. Kedzierski, A. Zielińska-Lipiec, J. Stępiński, S. Kac, J. Alloys Compd. 482 (2009) 114–117.
[9] T. Nagase, A. Yokoyama, Y. Umakoshi, J. Alloys Compd. 494 (2010) 295–300.
[10] J. He, H. Li, B. Yang, J. Zhao, H. Zhang, Z. Hu, J. Alloys Compd. 489 (2010) 535–540.
[11] H.J. Chang, W. Yook, E.S. Park, J.S. Kyeong, D.H. Kim, Acta Mater. 58 (2010) 2483–2491.
[12] T. Nagase, Y. Umakoshi, J. Alloys Compd. 505 (2010) L43–L46.
[13] T. Nagase, Y. Umakoshi, Intermetallics 18 (2010) 2136–2144.
[14] Y. Nakagawa, Acta Metall. 6 (1958) 704–711.
[15] K. Iwase, M. Okamoto, T. Amemiya, Sci. Rep. Tohoku Univ. 14 (1937) 618–640.
[16] P.A. Kindqvist, B. Uhrenius, Calphad 4 (1980) 193–200.
[17] Y. Chuang, R. Schmid, Y.A. Chang, Metall. Trans. A 15 (1984) 1921–1930.
[18] A. Munitz, Metall. Trans. 18B (1987) 565–575.
[19] S.P. Elder, A. Minutz, G.J. Abbaschian, Mater. Sci. Forum 50 (1989) 137–150.
[20] G. Wilde, R. Willnecker, R.N. Singh, F. Sommer: Z. Metallkd. 88 (1997) 804–809.
[21] G. Wilde, J.H. Perepezko, Acta Mater. 47 (1999) 3009–3021.
[22] S. Amara, A. Belhadj, R. Kersri, S.H. Thibaults, Z. Metallkd. 90 (1999) 116–123.
[23] R. Bhattacharya, B. Majumdar, K. Chattopadhyay, J. Electron Microsc. Suppl. 48 (1999) 1047–1054.
[24] X.Y. Lu, C.D. Cao, B. Wei, Mater. Sci. Eng. A 313 (2001) 198–206.
[25] C.P. Wang, X.J. Liu, I. Ohmura, R. Kainuma, K. Ishida, Science 297 (2002) 990–993.
[26] S. Bysakh, K. Chattopadhyay, T. Maiwald, R. Galun, B.L. Mordike, Mater. Sci. Eng. A 375–377 (2004) 661–665.
[27] K. Taguchi, H. Ono-Nakazto, T. Usui, ISIJ Int. 46 (2006) 29–32.
[28] T. Tanaka, T. Tagawa, Y. Asano, T. Tanaka, Netsusyori 41 (2001) 1–2 (in Japanese).
[29] T. Masumoto, Materials Science of Amorphous Metals, Ohm Publication, Tokyo, Japan, 1982.
[30] M. Naka, T. Masumoto, Sci. Rep. RITU A-27 (1979) 118–126.
[31] T. Nakajima, I. Nagami, H. Ino, J. Mater. Sci. Lett. 5 (1986) 60–62.